Journal of Materials Chemistry A

PAPER

View Article Online
View Journal | View Issue

Cite this: J. Mater. Chem. A, 2015, 3, 2378

Ionic conductivity of YSZ/CZO multilayers with variable lattice mismatch

Weida Shen*[a] and Joshua L. Hertz[ab]

Received 28th July 2014
Accepted 5th December 2014

DOI: 10.1039/c4ta03892d

www.rsc.org/MaterialsA

Heterostructured multilayers have been controversially reported to alter the oxygen ion conductivity of solid electrolytes by inducing interfacial mechanical strain. Here, we fabricated thin film multilayers composed of 9 mol% Y_2O_3 doped ZrO_2 (YSZ) and $Ce_{1-x}Zr_xO_2$ (CZO) to systematically quantify the effects of tensile strain on the oxygen-ion conduction behavior in YSZ. A significant advantage of using CZO is that its lattice parameter can be continuously varied by adjusting the Ce/Zr atomic ratio, simplifying the strain control over the neighboring YSZ layers. Three different sets of multilayers composed of YSZ with CeO_2, or with $Ce_{0.70}Zr_{0.30}O_2$ (CZO30), or with $Ce_{0.55}Zr_{0.45}O_2$ (CZO45) were prepared on Al_2O_3 substrates with interfacial lattice mismatch of +5.2%, +3.7%, and +2.9%, respectively. When decreasing the individual layer thicknesses from 35 nm to 5 nm, all of the multilayers exhibited little change of the conductivity, with values consistently near that of bulk YSZ. X-ray diffraction results indicate that the interfacial strains were largely relaxed. Suggestions that multilayers are unable to effect ionic conductivity changes must therefore consider the difficulties in obtaining lattice mismatch-based elastic strain, even at <3% mismatch.

1. Introduction

ZrO_2-based materials have been widely used as the electrolyte for solid oxide fuel cells (SOFCs) due in part to their very high mechanical and chemical durability.[1–3] The most representative and best known example is yttria-stabilized zirconia (YSZ).[4] Traditionally processed ceramic YSZ achieves sufficient oxygen ion conductivity (0.01 S cm^{-1}) for SOFC operation at temperatures over 800 °C.[1] This extremely high operating temperature decreases cell durability and increases component cost. In order to decrease the operating temperatures of SOFCs to 500 °C, one of the most important requirements is to increase the low temperature oxygen ion conductivity of the electrolyte. With the rapid development of thin film fabrication techniques, numerous recent reports have been focused on the study of nanostructured multilayers or heterostructures for solid electrolytes.[5–10] The unique interfacial effects between two oxides may have the capability to significantly alter the oxygen ion transport properties.

Azad *et al.* reported that conductivity increased by at least one order of magnitude in Gd_2O_3-doped ZrO_2/Gd_2O_3-doped CeO_2 multilayers as the thicknesses of the individual layers decreased to 15 nm.[11] Later studies by Sanna *et al.*[12] and Li *et al.*[13] observed similar increases in conductivity with increasing interfacial density in multilayers composed of YSZ with $Ce_{0.8}Sm_2O_{2-\delta}$ and YSZ with $Gd_2Zr_2O_7$, respectively. The defect concentration in the doped ZrO_2 and doped CeO_2 layers are relatively large such that any space charge regions at the multilayer interfaces are inconsequently small, approximately ≈1 Å.[14] Ion redistribution at the interfaces would thus have little impact on the overall defect concentrations or, therefore, oxygen ion conductivities. Instead, interfacial structures such as lattice mismatch strain were presumed to have altered the mobility of existing defects.

A systematic study of the effects of lattice mismatch strains on oxygen ion transport properties was reported previously.[15–18] Multilayers were composed of 9.5 mol% YSZ and various insulating rare earth oxides (*e.g.*, Y_2O_3, Lu_2O_3, and Sc_2O_3). Unlike the previous studies,[11–13] the rare earth oxides support little oxygen ion conductivity so that only the varying strain state in the YSZ layers would be expected to affect the measured oxygen ion conduction behavior of the multilayer structure. The interfacial conductivity of the structures was found to have a log-linear dependence on the amount of strain induced in the YSZ layers. Biaxial tensile strain in the YSZ layers increased the ionic conductivity, while compressive strain decreased it. This finding was in good agreement with a theoretical model based on the pressure dependence of the free energy for vacancy migration.

Other reports have suggested less effect from lattice-mismatched multilayers. Pergolesi *et al.* studied multilayers composed of YSZ and pure CeO_2 with a lattice mismatch of ≈+5% at interfaces.[19] The putative tensile strain induced in

[a]Department of Mechanical Engineering, University of Delaware, 126 Spencer Laboratory, Newark, DE 19716, USA. E-mail: weida@udel.edu; Fax: +1 302 831 3619; Tel: +1 302 831 8452

[b]Department of Materials Science and Engineering, University of Delaware, 201 DuPont Hall, Newark, DE 19176, USA

the YSZ, however, had no effect on the oxygen ion conduction, even when the individual layer thicknesses were decreased to 5 nm. Garcia-Barriocanal *et al.* claimed conductivity enhancement by eight orders of magnitude in YSZ/$SrTiO_3$ multilayers.[20] This increase was attributed to large tensile strain ($\approx$7%) in the YSZ layers, but evidence from ongoing experiments suggest that electronic conduction through the $SrTiO_3$ may be the true cause of the measured increases in total conductivity.[21–23]

In this work, we have fabricated multilayers composed of 9 mol% YSZ and $Ce_{1-x}Zr_xO_2$ (CZO) to study the ability to create tensile strain in YSZ-based multilayers. A significant advantage of using CZO as the strain-inducing material is that it has a lattice parameter that can be continuously varied by adjusting the Ce/Zr atomic ratio. CZO adopts cubic and/or tetragonal structures when the Zr content, x, is less than 0.5.[24–26] The lattice parameters of cubic and tetragonal CZO ($x \leq 0.5$) are nearly the same, such that the X-ray diffraction patterns of these phases are very difficult to distinguish.[26] The existence of tetragonal phase CZO does not affect its use as a means to create lattice mismatch. The similarity in crystal structure of CZO with YSZ increases the likelihood of creating epitaxial, coherently-strained multilayer thin films. Previous work by the authors developed a unique film fabrication method that provides compositional control within the Y_2O_3–ZrO_2–CeO_2 solid solution space at the single nanometer level.[27] This method was used recently to quantify a significant *reduction* in ionic conductivity with increasing biaxial *compression* in multilayers of CZO and yttria-doped ceria (YDC).[28] Here, we use highly analogous experimentation to examine if CZO can be used to create *increased* ionic conductivity *via* biaxial *tension* in neighboring YSZ layers.

2. Experimental

Thin films were reactively sputtered from single element targets of Ce, Zr, and Y (ACI Alloys, San Jose, CA) in a multi-target, magnetron sputtering machine (PVD Products, Wilmington, MA). Before film deposition, the main sputtering chamber was evacuated to a background pressure less than 1.33×10^{-5} Pa (10^{-7} Torr). Working gasses of Ar and O_2 were introduced into the sputtering chamber at a total flow rate of 20 sccm with an Ar/O_2 ratio of 9 : 1 and a working pressure of 1.33 Pa (10 mTorr). Single crystal Al_2O_3 (0001) substrates (10 mm $\times$ 10 mm $\times$ 0.5 mm) were heated to 650 °C for film growth. The details of the calibration of deposition rate and film composition were reported previously.[27]

Multilayer thin films were deposited using a software module controlling this sputtering system. Layers were sputtered sequentially with a control program that determined the power applied to each target and/or the toggling of desired target shutters. The details of characterization and verification of the multilayer structures were reported previously by the authors.[14]

The orientations of the films and their out-of-plane lattice parameters were characterized by θ–2θ X-ray diffraction (XRD) measurements in a Philip X'Pert diffractometer with Cu Kα radiation. Platinum interdigitated electrodes, as shown in Fig. 1, were fabricated on the surface of films by lift-off photolithography. The width and separation distance of the electrodes were each 100 μm with a total electrode perimeter length of $\approx$115 mm. Impedance spectra were measured in air using a Novocontrol Alpha-A analyzer with a signal voltage of 10 mV and frequency range between 1 Hz and 3 MHz. Before measurement, samples were first heated in air to 650 °C. The impedance data used to calculate the film conductivity were stable upon repeatedly cycling the temperature up to 650 °C and then measuring every 50 °C as the temperature decreased.

Recently, there is a concern of using electrodes deposited on the top surface of film to measure the resistance of the whole multilayer. Schweiger *et al.* used two different types of electrode structures to measure the electrical impedance of $Ce_{0.9}Gd_{0.1}O_{2-\delta}/Er_2O_3$ multilayers.[29] By using electrodes deposited on the side of the multilayers, the conductivity was found to be gradually decreased by at least one order of magnitude when the number of $Ce_{0.9}Gd_{0.1}O_{2-\delta}/Er_2O_3$ interfaces increased, but for the electrode pattern deposited on the top surface of the multilayers, the conductivity was nearly constant. Since the resistance of the Er_2O_3 layer was much larger compared to that of $Ce_{0.9}Gd_{0.1}O_{2-\delta}$, the electrical current was considered unable to penetrate into the whole multilayer for the electrodes deposited on the top surface and the current was blocked by the second insulating layer of Er_2O_3. The measured impedance was attributed to the electrical conduction through the top or the first $Ce_{0.9}Gd_{0.1}O_{2-\delta}$ layer, resulting similar effective conductivity even when the number of strained interfaces increased.

In this work, we used CZO as the second phase to induce different lattice mismatches at the interfaces between YSZ and CZO layers. The electrical conductivity of the rare earth oxides (*e.g.*, Y_2O_3, Gd_2O_3, and Er_2O_3) is much smaller. For example, at 727 °C, the electrical conductivity of Gd_2O_3 was only on the order of 10^{-6} S cm^{-1}.[30] On the other hand, the electrical conductivity of CZO was not so small and in the order of 10^{-4} S cm^{-1} at 650 °C.[31] This conductivity value was about 1.5 orders of magnitude less than that of YSZ at the same temperature. These CZO layers, therefore, are not so highly resistive as to block the current path from penetrating through the entire thickness of the multilayer. The current in this work was considered not to remain confined just to the top or the first layer of YSZ.

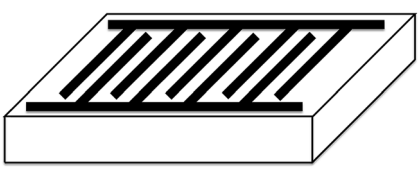

Fig. 1 Platinum interdigitated electrode pattern deposited on the top surface of film for impedance measurement. The width and inter-space of the electrode fingers were both kept at 100 μm. The total perimeter length of the electrodes was $\approx$115 mm.

3. Results and discussion

Three different sets of multilayers composed of 9 mol% YSZ with CeO_2, with $Ce_{0.70}Zr_{0.30}O_2$ (CZO30), or with $Ce_{0.55}Zr_{0.45}O_2$ (CZO45), were prepared. The lattice parameter of CZO obeys Vegard's law with a linear dependence on Zr content.[32] Based on the lattice parameters of YSZ ($\approx$5.14 Å (ref. 33)) and CeO_2 ($\approx$5.41 Å (ref. 34)), the lattice parameters of CZO30 and CZO45 solid solutions can be estimated as 5.33 Å and 5.29 Å, respectively. Since the lattice parameters of these CeO_2–ZrO_2 solid solutions are larger compared to that of YSZ, an in-plane tensile strain is ostensibly induced in YSZ layers near the interfaces in YSZ/CZO multilayers. The two constituent materials YSZ and CZO have closely related lattice symmetry, so the lattice mismatch at the interface, f, is calculated as

$$f = \frac{a_{CZO} - a_{YSZ}}{a_{YSZ}} \quad (1)$$

in which a denotes the lattice parameter.[15] Thus, the lattice mismatch is approximately +5.2% for YSZ/CeO_2, +3.7% for YSZ/CZO30, and +2.9% for YSZ/CZO45 multilayers. Based on reported measurements of YSZ and Gd_2O_3 doped CeO_2,[35] the Young's moduli of YSZ and CZO are presumed to be comparable, and thus one may assume that the lattice mismatch is borne as equal parts compressive strain in the CZO layer and tensile strain in the YSZ layer.

Ceria-based materials often exhibit polycrystalline structure on Al_2O_3 due to the large lattice mismatch between substrate and film.[36,37] On the other hand, YSZ films have exhibited nearly epitaxial growth on c-plane Al_2O_3 substrates in our previous work.[38] A 5 nm-thick YSZ was deposited first as a buffer layer to create epitaxial growth of the multilayer. The structure of the multilayer films can be described as

$$Al_2O_3—YSZ\ (5\ nm\text{-}thick)—CZO—(YSZ—CZO) \times N$$

in which N represents the number of YSZ/CZO bilayers. The total film thickness above the 5 nm-thick YSZ layer, as shown in Fig. 2, was constant at 105 nm, decreasing the individual layer thicknesses as needed to increase N. From Fig. 2, we can also see that each YSZ layer except the first 5 nm-thick buffer layer was sandwiched between two CZO layers, ensuring that only the YSZ/CZO interfaces (and not an air interface) would affect the measured oxygen ion conductivity. For each of the three sets of multilayers, three different samples were prepared, as described in Table 1. Four other single-layer thin films of YSZ, CeO_2, CZO30, and CZO45 with thickness of $\approx$105 nm were also prepared on Al_2O_3 substrates for comparison.

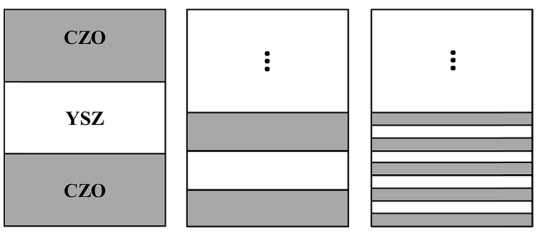

Fig. 2 Schematic structure of the multilayer films composed of alternating layers of YSZ and CZO above the 5 nm-thick YSZ buffer layer.

Fig. 3(a) shows the XRD patterns of the YSZ/CeO_2 multilayers on Al_2O_3 (0001) substrates. Single-layer YSZ and CeO_2 thin films with thickness of $\approx$105 nm are included for comparison. The single layer CeO_2 thin film exhibits both (111) and (100) orientations, but the single layer YSZ film and all of the YSZ/CeO_2 multilayers (which had the YSZ buffer layer) are highly textured along the (111) direction. The out-of-plane lattice parameters of YSZ and CeO_2 single-layer thin films calculated from the (111) diffraction locations were 5.21 Å and 5.41 Å, respectively. The lattice parameter of the CeO_2 thin film was almost the same as that of the bulk value, indicating that the film was fully relaxed on the Al_2O_3 substrate due to the very large lattice mismatch. For the single-layer YSZ thin film, the out-of-plane lattice parameter, however, exceeded the bulk value of 5.14 Å, an effect noted previously.[38] Since this value is larger than the bulk value by about 1.3%, a roughly 0.6% biaxial in-plane compressive strain (value estimated from an assumption of zero net lattice volume change) was presumed in the YSZ single-layer film due to the interface with the Al_2O_3 substrate.

For $N = 1$, the multilayer exhibits two separate diffraction peaks representing the planes of YSZ (111) and CeO_2 (111). The peak locations correspond to out-of-plane lattice parameters of 5.20 Å for YSZ and 5.44 Å for CeO_2. These values, therefore, represent a very slight reduction in lattice parameter for YSZ (111) and slight dilation for CeO_2 (111) in the out-of-plane direction. As the individual layer thickness decreased to 15 nm for the $N = 3$ multilayer, the peak locations did not significantly shift compared to the locations of $N = 1$. A superlattice pattern composed of an average structural peak SL_0 surrounded by two first-order satellite peaks SL_{-1} and SL_{+1} is observed for $N = 10$. The average lattice parameter based on the SL_0 peak was calculated to be 5.33 Å, which is in agreement with the average value of the out-of-plane lattice parameters of YSZ (5.20 Å) and CeO_2 (5.44 Å).

Fig. 3(b) shows the XRD patterns of the YSZ/CZO30 multilayers. The out-of-plane lattice parameter of the single-layer CZO30 film was calculated to be 5.35 Å, which was also slightly larger than that of the bulk material (5.33 Å). Similar to what was found in the YSZ/CeO_2 multilayers, the multilayer films exhibit (111) texture and transit from two distinct peaks to a superlattice pattern as the individual layer thicknesses decreased to 5 nm. For both the $N = 1$ and $N = 3$ multilayers, the out-of-plane lattice parameters were calculated to be 5.19 Å for YSZ and 5.42 Å for CZO30 (which was an increase from 5.35 Å for the CZO30 single layer film). These values again represent little effective mismatch strain created in the YSZ. For the $N = 10$ multilayer, the average lattice parameter based on the SL_0 peak was calculated to be 5.33 Å, which is again similar to the average value ($\approx$5.31 Å) of the out-of-plane lattice parameters of YSZ and CZO30.

The XRD patterns of the multilayers composed of YSZ and CZO45 are shown in Fig. 3(c). The out-of-plane lattice parameter of the single-layer CZO45 film was increased from 5.29 Å to 5.32 Å due to the substrate effect. For $N = 1$, the out-of-plane lattice

Table 1 Configuration of the samples within each of the three sets of multilayers

Sample	CZO layer thickness (nm)	YSZ layer thickness (nm)	Number of bilayers (N)
$N = 1$	35	35	1
$N = 3$	15	15	3
$N = 10$	5	5	10

parameter for YSZ was calculated to 5.19 Å, the same as that in YSZ/CZO30 multilayer. The lattice parameter of CZO45 in the multilayer film was 5.35 Å, an increase from 5.32 Å as a single-layer film. The two peaks start to transition to a superlattice pattern for the $N = 3$ multilayer. In this sample, the lattice parameter based on the CZO45 peak increased to 5.38 Å, but the value for YSZ remained 5.19 Å. A strong superlattice pattern is found for the $N = 10$ multilayer. The average lattice parameter calculated based on the SL_0 peak was 5.29 Å, which is again similar to the computed average of the lattice parameters of the constituent layers, YSZ and CZO45.

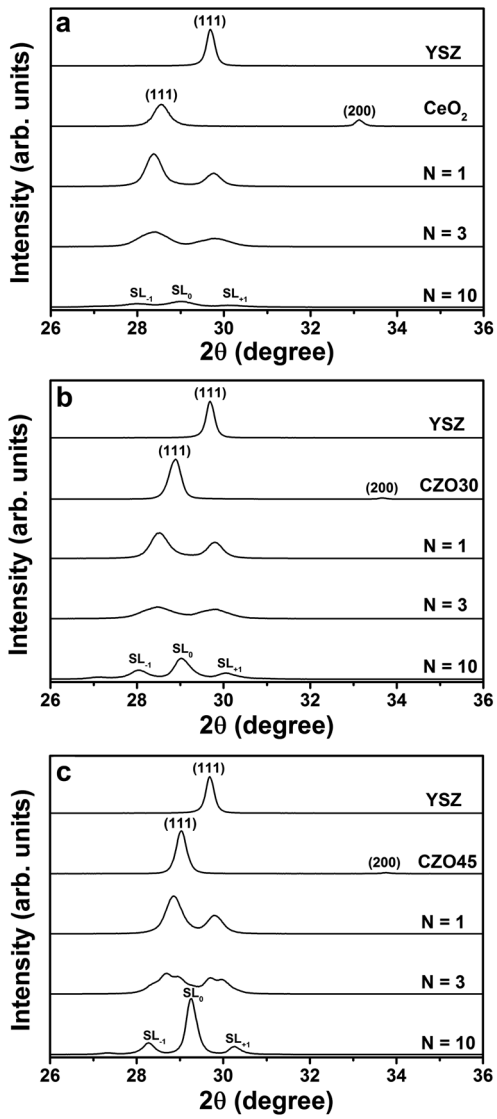

Fig. 3 XRD patterns of multilayer thin films composed of N bilayers of (a) YSZ and CeO_2, (b) YSZ and CZO30, and (c) YSZ and CZO45. The corresponding single-layer YSZ and CZO thin films deposited on Al_2O_3 (0001) with thickness of ≈105 nm were also included for comparison.

Table 2 compares the out-of-plane lattice parameters of YSZ and CZO in bulk, single-layer films, and $N = 1$ and $N = 3$ multilayers. The bulk lattice parameters for CZO30 and CZO45 were calculated based on the Vegard's law, as discussed before. The out-of-plane lattice parameters of the YSZ across all three sets of multilayers were very similar to that of the single-layer film, ranging between 5.20 Å and 5.19 Å. The coupling of CZO with YSZ has insignificant effects on the YSZ lattice parameter. Thus, the interfacial strains in YSZ layers in YSZ/CZO multilayers were largely or fully relaxed. At the same time, the out-of-plane lattice parameters of the CZO gradually increased from the single-layer films to the $N = 1$ and $N = 3$ multilayers. Similar to the substrate effect noted previously for YSZ, the single-layer CZO30 and CZO45 films exhibited larger out-of-plane lattice parameters compared to that of the bulk materials. The single layer CeO_2 film had a lattice parameter that matched the bulk value. By increasing the bilayer number from $N = 1$ to $N = 3$, the out-of plane lattice parameters of the CZO all gradually increased. These results indicate that the creation of tensile strains in the YSZ layers was much more difficult compared to the creation of compressive strains in the CZO layers.

Previous work by the authors on multilayers of YDC and CZO found that as the individual layer thickness decreased, a superlattice diffraction pattern appeared and then, upon further thickness reduction to 5 nm, almost gave way to a single, sharp, very high-intensity peak.[28] This indicated that the whole multilayer could be characterized by a single lattice parameter and that the YDC layers were effectively being compressively strained from the CZO layers. In this work, two distinct peaks remain for the $N = 3$ multilayers, and a superlattice pattern remains with satellite peaks clearly identified for the $N = 10$ multilayers. These results give clear indication that two distinct lattice parameters remain even for the thinnest individual layer thickness of 5 nm.

Table 2 The lattice parameters of YSZ and CZO in the bulk, single-layer films, and $N = 1$ and $N = 3$ YSZ/CZO multilayers

	YSZ/CeO2		YSZ/CZO30		YSZ/CZO45	
Sample	YSZ	CeO_2	YSZ	CZO30	YSZ	CZO45
Bulk	5.14 Å	5.41 Å	5.14 Å	5.33 Å	5.14 Å	5.29 Å
Single layer	5.21 Å	5.41 Å	5.21 Å	5.35 Å	5.21 Å	5.32 Å
$N = 1$	5.20 Å	5.44 Å	5.19 Å	5.42 Å	5.19 Å	5.35 Å
$N = 3$	5.20 Å	5.45 Å	5.19 Å	5.43 Å	5.19 Å	5.38 Å

Moreover, the appearance of clear and sharp satellite peaks indicates the formation of high-quality, well-defined interfaces between the constituent layers.[12] Nevertheless, the intensity of the SL_0 peak of the YSZ/CeO_2 $N = 10$ multilayer is much smaller than that of the corresponding YSZ/CZO30 and YSZ/CZO45 multilayers, indicating relatively rougher or otherwise less ideal interfaces where the lattice mismatch is very large. The satellite peak angular locations allow direct calculation of the bilayer thickness according to

$$\Lambda = \frac{\lambda_{Cu}}{\sin\theta_{+1} - \sin\theta_{-1}} \quad (2)$$

in which Λ represents the bilayer thickness, λ_{Cu} denotes the wavelength of Cu Kα radiation (1.5418 Å), and θ_{+1} and θ_{-1} are the angular positions of satellite peaks SL_{+1} and SL_{-1}, respectively.[12] Based on this equation, the bilayer thicknesses of the $N = 10$ multilayers composed of YSZ with CeO_2, CZO30, and CZO45 were calculated to be 8.7 nm, 9.1 nm and 9.2 nm, respectively. These values are very close to the values of 10.4 nm, 10.7 nm, and 10.4 nm calculated from the total film thickness as measured by interferometry and the known number of constituent layers.

Fig. 4 shows typical impedance spectra, from a YSZ/CZO45 ($N = 10$) multilayer at three different temperatures. At each temperature, the spectrum consists of a semicircle at high frequency and the beginning of a second semicircle at low frequency. Two R-CPE elements connected in series were used as the equivalent circuit to fit the impedance spectra. An additional resistance, R_{YSZ}, in the equivalent circuit represents the resistance of the 5 nm-thick YSZ buffer layer. The value of R_{YSZ} was fixed at each temperature and calculated based on the electrode geometry and conductivities obtained from a single layer YSZ thin film ($\approx$105 nm). Resistance R_{YSZ} was always at least one order of magnitude greater than $R1$. The equivalent capacitance of the constant phase element for the high frequency semicircle, CPE1, was found to be of order 10^{-11} F. This value is as low as can be measured in the experimental setup, and represents a stray capacitance in parallel with the sample under test. The equivalent capacitance value of CPE2 for the low frequency semicircle was at least four orders of magnitude larger, which is much too large to be due to conduction between the electrodes. This result clearly indicates that resistance $R1$ was due to conduction through the film eliminating the contribution from the 5 nm-thick YSZ buffer layer, while $R2$ was due to electrode polarization.

Fig. 5 shows the fitted resistance of $R1$ as a function of the individual layer thickness in YSZ/CZO30 multilayers at 650 °C. As mentioned before, for electrodes deposited on the top surface of film, there is a concern of measuring just the impedance of the first YSZ layer. If we assume this concern is true, then as the top layer thickness of YSZ decreased from 35 nm to 5 nm in the multilayers, the fitted resistance of $R1$ for the whole multilayers needs to be gradually increased. The measured resistance for the multilayers with 5 nm-thick YSZ should be 3 times larger than that in multilayers with 15 nm-thick YSZ, and 7 times larger than that in multilayers with 35 nm-thick YSZ. In reality, as shown in Fig. 5, the fitted resistance of $R1$ was nearly constant when the individual thickness decreased from 35 nm to 5 nm. For the other two types of multilayers composed of YSZ with CeO_2 or with CZO45, the fitted resistance $R1$ was also found to be essentially independent of the individual layer thickness. These findings indicated that the measurement current was not just confined to the top or the first YSZ layer, but penetrating into the whole multilayer.

The undoped CeO_2 possesses relatively low oxygen ion conductivity, on the order of 10^{-3} at 650 °C.[39] The addition of Zr into CeO_2 to form CZO further decreases the conductivity due to the reduced vacancy mobility.[40] The electrical conductivity of the CZO, therefore, is at least one order of magnitude less compared to that of YSZ. The contributions from the CZO and 5 nm thick YSZ buffer layer to the overall electrical conduction can be likely neglected. The overall conductivity of the multilayers in this work, σ, was calculated based on $R1$, the electrode geometry, and the total thickness of YSZ within the multilayer according to the equation of

$$\sigma = \frac{w}{R1 \times (L \times t)} \quad (3)$$

in which w represents the inter-space between two electrode fingers ($w = 100$ μm), L represents the thickness of YSZ layers

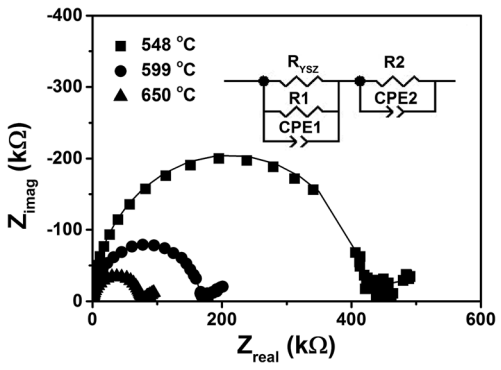

Fig. 4 Impedance spectra measured in open air of YSZ/CZO45 multilayers with $N = 10$ at the temperatures indicated. Also shown is the equivalent circuit used to fit the data (R_{YSZ} was a fixed value at each temperature).

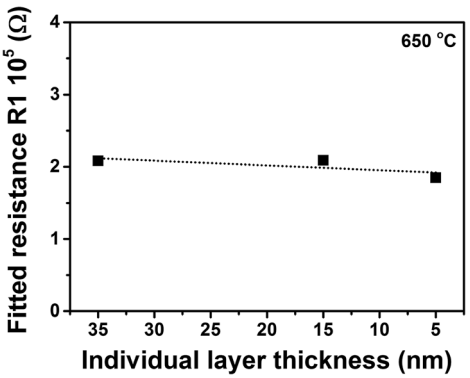

Fig. 5 The fitted resistance $R1$ of YSZ/CZO30 multilayers as a function of the individual layer thickness at 650 °C.

within the multilayer, t denotes the total perimeter length of the electrodes ($t \approx 115$ mm).

Fig. 6 compares the oxygen ion conductivity of the 105 nm-thick YSZ single-layer film studied in this work with a single YSZ substrate measured in our lab. The activation energies (determined from the σT product) are also included in the figure. The Y_2O_3-dopant concentration in these two materials was similar, about 8–9 mol%. The conductivity of the single-layer film was found to be about 0.25 orders of magnitude less compared to that of the single crystal. One of the possible causes for the decreased conductivity for the YSZ thin film may be due to the compressive strain exerted by the substrate, as discussed in the XRD analysis. Moreover, the single-layer and multilayer YSZ films likely adopted a columnar microstructure. Grain boundaries are well known to depress ionic conductivity in YSZ.

The single layer and multilayer YSZ films are believed to have adopted similar columnar structures, and thus any effects of the existence of grain boundaries would be felt across all of the measured films. It is possible that the effects of tensile strain that we seek to find in this study could be masked by a grain boundary conductivity that is both very low and unaffected by strain. However, no such difficulties plagued the previous, highly parallel study in ref. 28, where both grain boundaries and strain effects were conclusively found.

Fig. 7(a) shows Arrhenius plots of the electrical conductivity of YSZ/CeO_2 multilayers measured in air. The conductivity of a single layer YSZ thin film with thickness of ≈105 nm is included for comparison. From the figure, we can see that the electrical conductivities for $N = 1$ and $N = 3$ have similar values compared to that of the YSZ thin film. The electrical conductivity for $N = 10$, however, is slightly reduced by a factor of ≈2. These results compare very well to those reported by Pergolesi *et al.*[19] on a similar study of multilayers composed of YSZ and CeO_2. In that study, the authors found no change in conductivity of YSZ even with individual layer thickness decreased to 5 nm. The slightly decreased conductivity for $N = 10$ in this work, similar to what was found in our previous study of YDC/CeO_2 multilayers, may be due to non-zero roughness at the interfaces.[28] As shown in Fig. 3, the YSZ/CZO multilayers with smallest layer thicknesses exhibited typical superlattice XRD patterns consisting of an average diffraction peak SL_0 surrounded by two satellite peaks SL_{+1} and SL_{-1}. The appearance of clear and sharp satellite peaks indicates the formation of high-quality, well-defined interfaces between two constituent layers. The intensity of the satellite peaks of the YSZ/CeO_2 multilayer for $N = 10$, however, were much smaller, broader, and less well defined than that of the corresponding YSZ/CZO30 and YSZ/CZO45 multilayers. All of these findings support our conclusion that the YSZ/CeO_2 interfaces were relatively rougher, likely due to the very large lattice mismatch.

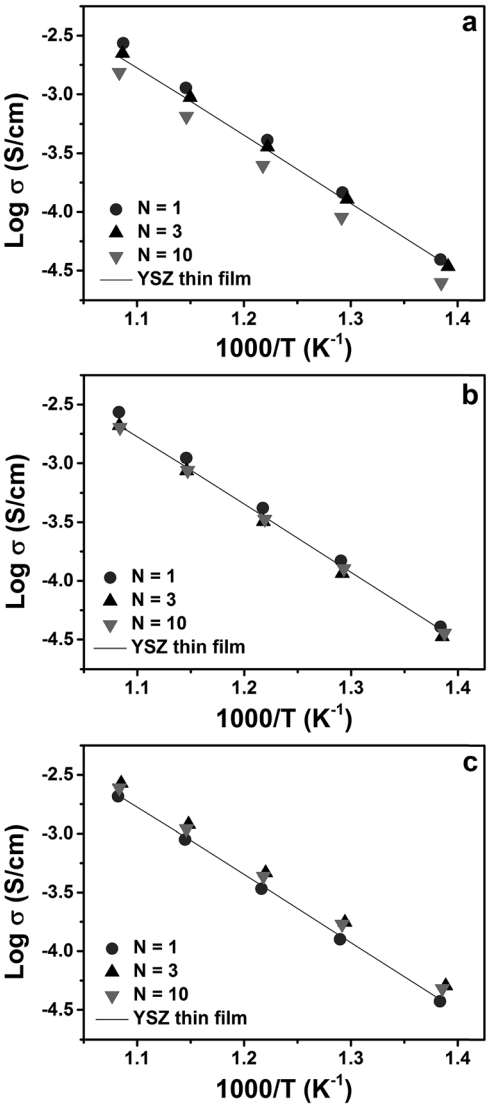

Fig. 7 Arrhenius plots of the electrical conductivity of the YSZ layers in the (a) YSZ/CeO_2, (b) YSZ/CZO30, and (c) YSZ/CZO45 multilayers. Shown for comparison is the conductivity measured from a single-layer YSZ film with thickness of ≈105 nm.

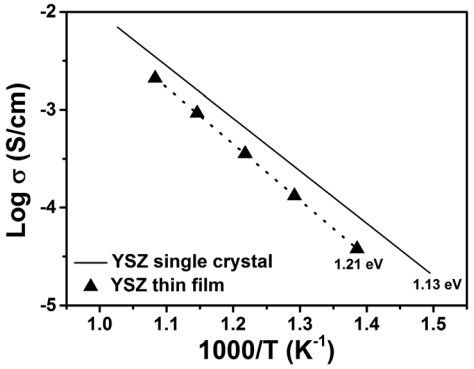

Fig. 6 Comparison of electrical conductivity between a 105 nm-thick YSZ single-layer film and a roughly 500 μm-thick single crystal YSZ bulk sample.

Fig. 7(b) and (c) show Arrhenius plots of electrical conductivity of the YSZ/CZO30 and YSZ/CZO45 multilayers, respectively. In both cases, as the individual layer thickness decreased from 35 nm ($N = 1$) to 5 nm ($N = 10$), the multilayers exhibit nearly identical conductivities as that of the YSZ single-layer

thin film. The decreased interfacial lattice mismatch in these multilayers relative to the YSZ/CeO_2 multilayers seems to increase the interface quality for $N = 10$, resulting in similar conductivities with those of the $N = 1$ and $N = 3$ multilayers.

The conduction behavior of the multilayers can be better understood by deconvoluting the conduction paths through the YSZ layers into two independent, parallel parts.[41] The first pathway is through the volume or bulk region, and the second pathway is through the region close to the interface. The relationship between the total conductivity and the volume and interfacial conductivities is derived as[41]

$$\sigma_{tot} = \sigma_{vol} + 2\delta(\sigma_{int} - \sigma_{vol})\frac{1}{d} \quad (4)$$

in which σ_{tot} represents te total conductivity of the multilayer, σ_{vol} denotes the volume conductivity, σ_{int} represents the interfacial conductivity, δ represents the thickness of the interfacial region, and d is the layer thickness of the YSZ. From the equation, it can be seen that the total conductivity is linearly dependent on the reciprocal thickness $1/d$ when $d \geq 2\delta$. For $d < 2\delta$, the total conductivity is only determined by the interfacial regions.

Fig. 8 shows conductivity isotherms at 650 °C for the three sets of multilayers as a function of the reciprocal layer thickness. Based on eqn (4), a linear fit of the total conductivity as a function of $1/d$ allows us to deconvolute the volume and interfacial conductivities. In our previous study of YDC/CZO multilayers, the total conductivity reduced in a roughly log-linear fashion as the individual layer thickness decreased to 5 nm, and so the interfacial region was assumed to be around 2.5 nm thick.[28] We assume here that the thickness of the interfacial region is again 2.5 nm. At each temperature, the volume and interfacial conductivities can therefore be calculated.

Fig. 9 shows Arrhenius plots of the calculated volume or bulk and interfacial conductivities of the multilayers. The volume conductivities of each of the multilayers are highly similar to each other and to the total conductivity of the single-layer YSZ thin film. This result is intuitively expected, since the volume regions were thought to be unaffected by the interfaces. Fig. 9(a) compares the volume and interfacial conductivities in the YSZ/CeO_2 multilayers. The interfacial conductivity is smaller by about a factor of ≈2. As mentioned before, this decreased conductivity may be due to interfacial roughness related to the very large lattice mismatch. As shown in Fig. 9(b) and (c), the volume and interfacial conductivities of the YSZ/CZO30 and YSZ/CZO45 multilayers are all nearly the same as the conductivity of a YSZ single-layer film. There is a correlation of increased interfacial conductivity as the zirconia content of the CZO layer is reduced (*i.e.*, as the lattice mismatch with YSZ is reduced), though the changes are sufficiently small that this may be due to chance.

In Korte *et al.*'s investigation of multilayers composed of YSZ and Y_2O_3, interfacial lattice mismatch of ≈+3% correlated to significant increases in conductivity.[15] The total conductivity gradually increased by a factor of about 2 as the YSZ layer

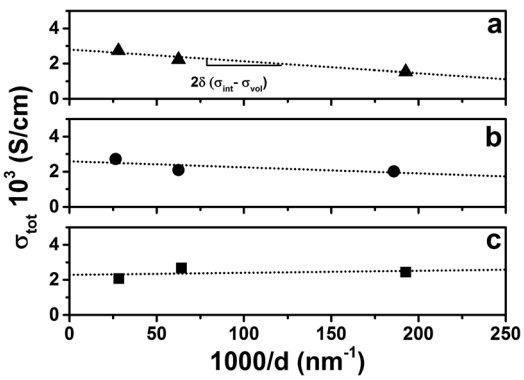

Fig. 8 Conductivity isotherms at 650 °C of (a) YSZ/CeO_2, (b) YSZ/CZO30, and (c) YSZ/CZO45 multilayers as a function of the reciprocal thickness of the YSZ layers, $1/d$.

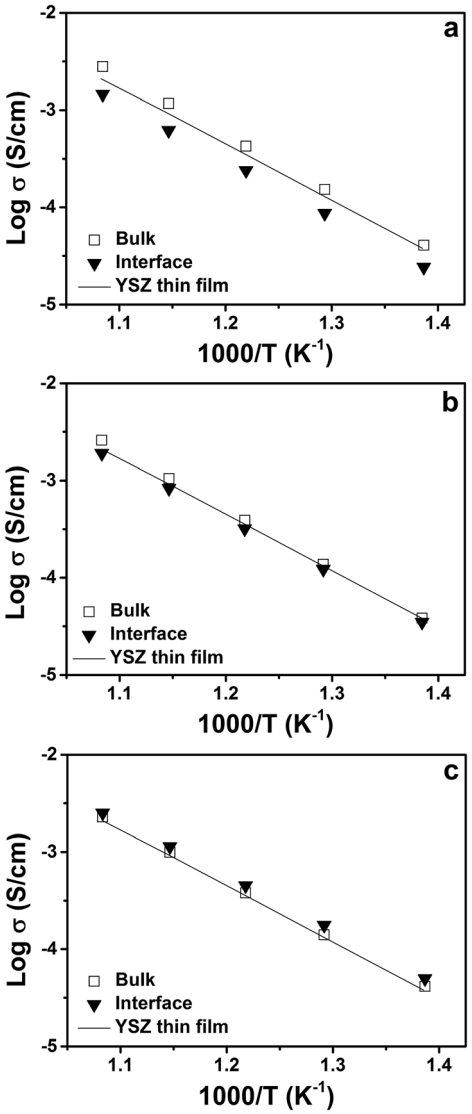

Fig. 9 The calculated volume (bulk) and interfacial conductivities for three different types of multilayers of (a) YSZ/CeO_2, (b) YSZ/CZO30, and (c) YSZ/CZO45 as a function of temperature. The YSZ thin film data comes from measurements of a single layer film with thickness of ≈105 nm.

thickness decreased from 526 nm to 24 nm. At the same time, the activation energy decreased from 1.13 eV to 0.99 eV, suggesting that the strain was effectively increasing vacancy mobility. Li *et al.* studied multilayers composed of YSZ and $Gd_2Zr_2O_7$, which has a similar lattice mismatch of +3% compared to the YSZ/Y_2O_3 multilayers.[13] A key difference with this type of multilayers is that, unlike Y_2O_3, $Gd_2Zr_2O_7$ is an oxygen ion conductor. There is thus the risk of a convolution of lattice mismatch strain-based effects, with the conducting phase on one side of the interface being compressed simultaneously with the conducting phase on the other side of the interface being expanded. Nevertheless, Li *et al.* reported that the +3% lattice mismatch caused the oxygen ion conductivity to increase by 2 orders of magnitude relative to bulk YSZ when the layer thickness decreased to 5 nm. The increased conductivity was attributed to the coherent, dislocation-free interfaces between YSZ and $Gd_2Zr_2O_7$, imposing large tensile strain on YSZ layers.

In this work, we studied three different types of YSZ/CZO multilayers, but the tensile lattice mismatch caused very little effect on the oxygen ion transport properties. The XRD patterns shown in Fig. 2 indicate that the out-of-plane lattice parameters for YSZ were essentially unaffected across the range of lattice mismatch magnitudes and layer thicknesses employed in this study. The >+5% lattice mismatch between YSZ and pure CeO_2 makes it likely that the strain was released by the creation of non-coherent interfaces in these multilayers. It is not surprising then that, as in ref. 19, no change in conductivity was measured.

The YSZ/CZO45 multilayers possess similar lattice mismatch as the YSZ/Y_2O_3 (ref. 15) and YSZ/$Gd_2Zr_2O_7$ (ref. 13) multilayers. It is more surprising that no change in conductivity was measured in the YSZ/CZO45 multilayers, since the (ref. 13 and 15) suggest that YSZ was capable of accommodating this magnitude of lattice mismatch strain. Thus, we conclude that lattice mismatch strains of ≈+3% are close to a maximum practically achievable limit for YSZ, with the creation of coherent interfaces dependent on processing details. Continued research with high resolution transmission electron microscopy would enable visualization of the mechanism behind the strain relaxation. Based on the results discussed here, the insignificant effect of tensile lattice mismatch on the oxygen ion conductivity is due to strain relaxation even at "low" values of lattice mismatch and is *not* due to the lack of a mechano-electrochemical coupling effect. Reports of significantly greater tensile strains being accommodated in YSZ, therefore, must be treated with caution. Results from multilayers composed of doped ZrO_2 and doped CeO_2 that have been reported in the literature[11,12] (*e.g.*, YSZ and $Ce_{0.8}Sm_2O_{2-\delta}$) suggested that significant increase in conductivity can be derived due to >+5% lattice mismatch. It is difficult to believe that such large tensile strains could be accommodated in YSZ.

4. Conclusion

In this work, we studied the effects of tensile lattice mismatch on oxygen ion conductivity in multilayers composed of YSZ with CeO_2, CZO30, and CZO45 with layer thicknesses ranging between 5 nm and 35 nm. Very little conductivity change was found in the multilayers, with values near that of bulk YSZ. Based on the calculated out-of-plane YSZ lattice parameters and the strong superlattice peaks in the diffraction patterns, it is believed that the lattice mismatch strain in the multilayers has been relaxed by the creation of incoherent interface structures. For YSZ/CZO45 multilayers, the lattice mismatch of +2.9%, is very similar as that of previously reported YSZ/Y_2O_3 multilayers, suggesting that biaxial strains of this magnitude represent a rough upper practical limit.

Acknowledgements

Research supported by the U.S. Department of Energy, Office of Basic Energy Sciences, Division of Materials Sciences and Engineering under Award DE-SC0005403.

References

1 B. C. H. Steele and A. Heinzel, *Nature*, 2001, **414**, 345–352.
2 Y. Arachi, H. Sakai, O. Yamamoto, Y. Takeda and N. Imanishai, *Solid State Ionics*, 1999, **121**, 133–139.
3 F. M. L. Figueiredo and F. M. B. Marques, *WIREs Energy Environ.*, 2013, **2**, 52–72.
4 N. Q. Minh, *J. Am. Ceram. Soc.*, 1993, **76**, 563–588.
5 E. Fabbri, D. Pergolesi and E. Traversa, *Sci. Technol. Adv. Mater.*, 2010, **11**, 054503.
6 J. Maier, *Nat. Mater.*, 2005, **4**, 805–815.
7 S. Ramanathan, *J. Vac. Sci. Technol., A*, 2009, **27**, 1126–1134.
8 X. X. Guo and J. Maier, *Adv. Mater.*, 2009, **21**, 2619–2631.
9 J. Garcia-Barriocanal, A. Rivera-Calzada, M. Varela, Z. Sefrioui, M. R. Diaz-Guillen, K. J. Moreno, J. A. Diaz-Guillen, E. Iborra, A. F. Fuentes, S. J. Pennycook, C. Leon and J. Santarnaria, *ChemPhysChem*, 2009, **10**, 1003–1011.
10 X. Guo, *Scr. Mater.*, 2011, **65**, 96–101.
11 S. Azad, O. A. Marina, C. M. Wang, L. Saraf, V. Shutthanandan, D. E. McCready, A. El-Azab, J. E. Jaffe, M. H. Engelhard, C. H. F. Peden and S. Thevuthasan, *Appl. Phys. Lett.*, 2005, **86**, 131906.
12 S. Sanna, V. Esposito, A. Tebano, S. Licoccia, E. Traversa and G. Balestrino, *Small*, 2010, **6**, 1863–1867.
13 B. Li, J. M. Zhang, T. Kaspar, V. Shutthanandan, R. C. Ewing and J. Lian, *Phys. Chem. Chem. Phys.*, 2013, **15**, 1296–1301.
14 W. D. Shen, J. Jiang, C. Y. Ni, Z. Voras, T. P. Beebe and J. L. Hertz, *Solid State Ionics*, 2014, **255**, 13–20.
15 C. Korte, A. Peters, J. Janek, D. Hesse and N. Zakharov, *Phys. Chem. Chem. Phys.*, 2008, **10**, 4623–4635.
16 C. Korte, N. Schichtel, D. Hesse and J. Janek, *Monatsh. Chem.*, 2009, **140**, 1069–1080.
17 N. Schichtel, C. Korte, D. Hesse and J. Janek, *Phys. Chem. Chem. Phys.*, 2009, **11**, 3043–3048.
18 N. Schichtel, C. Korte, D. Hesse, N. Zakharov, B. Butz, D. Gerthsen and J. Janek, *Phys. Chem. Chem. Phys.*, 2010, **12**, 14596–14608.
19 D. Pergolesi, E. Fabbri, S. N. Cook, V. Roddatis, E. Traversa and J. A. Kilner, *ACS Nano*, 2012, **6**, 10524–10534.

20 J. Garcia-Barriocanal, A. Rivera-Calzada, M. Varela, Z. Sefrioui, E. Iborra, C. Leon, S. J. Pennycook and J. Santamaria, *Science*, 2008, **321**, 676–680.
21 X. Guo, *Science*, 2009, **324**, 465.
22 J. Garcia-Barriocanal, A. Rivera-Calzada, M. Varela, Z. Sefrioui, E. Iborra, C. Leon, S. J. Pennycook and J. Santamaria, *Science*, 2009, **324**, 465.
23 A. Cavallaro, M. Burriel, J. Roqueta, A. Apostolidis, A. Bernardi, A. Tarancon, R. Srinivasan, S. N. Cook, H. L. Fraser, J. A. Kilner, D. W. McComb and J. Santiso, *Solid State Ionics*, 2010, **181**, 592–601.
24 C. E. Hori, H. Permana, K. Y. S. Ng, A. Brenner, K. More, K. M. Rahmoeller and D. Belton, *Appl. Catal., B*, 1998, **16**, 105–117.
25 Y.-P. Fu, S.-H. Hu and B.-L. Liu, *Ceram. Int.*, 2009, **35**, 3005–3011.
26 M. Kuhn, S. R. Bishop, J. L. M. Rupp and H. L. Tuller, *Acta Mater.*, 2013, **61**, 4277–4288.
27 J. Jiang, W. D. Shen and J. L. Hertz, *Thin Solid Films*, 2012, **522**, 66–70.
28 W. Shen, J. Jiang and J. L. Hertz, *RSC Adv.*, 2014, **4**, 21625–21630.
29 S. Schweiger, M. Kubicek, F. Messerschmitt, C. Murer and J. L. M. Rupp, *ACS Nano*, 2014, **8**, 5032–5048.
30 C. D. Wirkus, M. F. Berard and D. R. Wilder, *J. Am. Ceram. Soc.*, 1969, **52**, 456.
31 M. Boaro, A. Trovarelli, J. H. Hwang and T. O. Mason, *Solid State Ionics*, 2002, **147**, 85–95.
32 G. R. Rao and H. R. Sahu, *Proc.–Indian Acad. Sci., Chem. Sci.*, 2001, **113**, 651–658.
33 H. Yamane and T. Hirai, *J. Cryst. Growth*, 1989, **94**, 880–884.
34 M. O'Connell and M. A. Morris, *Catal. Today*, 2000, **59**, 387–393.
35 A. Atkinson and A. Selcuk, *Solid State Ionics*, 2000, **134**, 59–66.
36 I. Kosacki, T. Suzuki, V. Petrovsky and H. U. Anderson, *Solid State Ionics*, 2000, **136**, 1225–1233.
37 T. Suzuki, I. Kosacki and H. U. Anderson, *Solid State Ionics*, 2002, **151**, 111–121.
38 J. Jiang, X. Hu, W. Shen, C. Ni and J. L. Hertz, *Appl. Phys. Lett.*, 2013, **102**, 143901.
39 I. Kosacki, T. Suzuki, V. Petrovsky and H. U. Anderson, *Solid State Ionics*, 2000, **136–137**, 1225–1233.
40 V. Ruhrup and H. D. Wiemhofer, *Z. Naturforsch., B: J. Chem. Sci.*, 2006, **61**, 916–922.
41 A. Peters, C. Korte, D. Hesse, N. Zakharov and J. Janek, *Solid State Ionics*, 2007, **178**, 67–76.